Petroleum Science 23 (2026) 1293–1306

Contents lists available at ScienceDirect

Petroleum Science

journal homepage: www.keaipublishing.com/en/journals/petroleum-science

Original Paper

# A micro-crosslinked amphiphilic copolymer viscosifier for high temperature and high-density inorganic salt completion fluids

Kai-He Lv [a], Qiang Li [a], Li-Li Yan [c], Yong Kong [d], Zhang-Cheng Yang [e], Yuan-Zhi Qu [c], Ren Wang [c], Jin-Sheng Sun [a,b,c], Jian Li [a,b,*]

[a] School of Petroleum Engineering, China University of Petroleum (East China), Qingdao, 266580, Shandong, China
[b] State Key Laboratory of Deep Oil and Gas, China University of Petroleum (East China), Qingdao, 266580, Shandong, China
[c] CNPC Engineering Technology R&D Company Limited, Beijing, 102206, China
[d] Sinopec Dezhou Continental Shelf Petroleum Engineering Technology Co., Ltd, Dezhou, 253011, Shandong, China
[e] China National Petroleum Corporation Tarim Oilfield Branch, Kuerle, 841000, Xinjiang, China

ARTICLE INFO

*Article history:*
Received 4 July 2025
Received in revised form
25 November 2025
Accepted 26 November 2025
Available online 29 November 2025

Edited by Jia-Jia Fei

*Keywords:*
Solid-free completion fluids
Viscosifier
High temperature and high density
Calcium bromide
Deep and ultra-deep wells

ABSTRACT

Solid-free brine completion fluids, characterized by their exceptional reservoir protection capabilities and optimal rheological behavior, are highly desirable for applications in oil and gas reservoirs and have attracted significant attention in recent decades. However, as the core component of completion fluids, the viscosifier was prone to curling or even precipitating in high-temperature, high-density inorganic salt (divalent calcium) environments, leading to failure in thickening performance. In this study, a micro-crosslinked amphoteric viscosifier (i.e., A-DDAS) resistant to high temperature and calcium ions was synthesized via free radical copolymerization of N,N-dimethylacrylamide (DMAA), diallyl dimethyl ammonium chloride solution (DMDAAC), 2-acrylamido-2-methylpropane sulfonic acid (AMPS), [2-(methacryloyloxy) ethyl] dimethyl-(3-sulfopropyl) ammonium hydroxide (SBMA), and pentaerythritol triallyl ether (APE). The molecular structure and physicochemical properties of the copolymer were systematically studied by NMR, FTIR, XPS, TGA and XRD. Rheological experiments demonstrated that calcium bromide brine containing A-DDAS copolymers exhibited outstanding shear-thinning behavior and rapid thixotropic recovery, essential for efficient wellbore cleaning and fluid displacement during completion operations. As the density of calcium bromide brine increased, more calcium ions shield electrostatic attractions between the cationic and anionic moieties along the copolymer backbone, thereby promoting full extension of the polymer chains and enhancing the binding energy with water molecules. After adding 1.0 wt% A-DDAS copolymer to a 1.75 g/cm$^3$ calcium bromide brine and aging the mixture at 180 °C for 16 h, the completion fluids exhibited an apparent viscosity of 71 mPa·s, plastic viscosity of 64 mPa·s, and yield point of 7 Pa, which were significantly better than common viscosifiers (HE300 and Dristemp). Therefore, A-DDAS copolymers demonstrated exceptional thickening capacity and dynamic shear enhancement in high-temperature, high-density calcium bromide brine, notably rendering it ideally suited for deployment in completion fluids for deep and ultra-deep wells.


## 1. Introduction

Oil and natural gas are the material basis for human production and life and will remain the world's main sources of energy consumption until 2050 (Li et al., 2022a). With the gradual depletion of conventional shallow oil and gas resources, deep and unconventional formations have become the primary focus of oil and gas exploration and development (Li et al., 2022b). Completion engineering refers to the final process in the drilling of oil and gas wells, which connects the bottom of the well and the reservoir in a certain way, thereby forming a channel for oil and gas to flow from the reservoir to the surface (Singh et al., 2023). The completion fluids composed of water, solid particles, chemical additives, etc., have the functions of balancing formation pressure, reducing reservoir damage, suspending rock debris, and maintaining

* Corresponding author.
*E-mail address:* cuplijian@sina.com (J. Li).
Peer review under the responsibility of China University of Petroleum (Beijing).

https://doi.org/10.1016/j.petsci.2025.11.046

downhole cleanliness, which is crucial for oil and gas production (Kazemihokmabad et al., 2024). According to whether the completion fluids contain solid particles, they can be divided into solid-phase completion fluids (SCF) and non-solid-phase completion fluids (NSCF). SCF can achieve large-scale density regulation, avoid rock debris precipitation, and prevent fluids invasion into the formation by adding solid particles (bentonite, limestone, barite, etc) in different proportions, which is commonly used for the completion of high-pressure and collapse-prone formations. However, under the pressure difference between the liquid column in the well and the formation pressure, solid particles in SCF are easily able to enter the pores and throats of the reservoir, forming bridges and blockages, resulting in a significant decrease in oil and gas production (Khan et al., 2022; Tariq et al., 2020). As a control, NSCF configured with soluble organic/inorganic salts has low damage, good flowability, and is easy to configure and maintain, making it the mainstream direction of current well-completion fluids technology development (Jia et al., 2019). Organic salt completion fluids mainly composed of formate salts (such as sodium formate, cesium formate, etc.), phosphates, ammonium salts, etc., have the advantages of low corrosiveness and high biodegradability, but their high price and poor high-temperature stability limit their large-scale promotion and application. Fortunately, NSCF composed of inorganic salts (sodium chloride, calcium chloride, calcium bromide, etc.) has low cost and good high-temperature stability, making it suitable for large-scale oil and gas development operations (Rana et al., 2024; Singh et al., 2024).

As the core additive used in well completion fluids, viscosities can form a three-dimensional network structure through hydrogen bonding, electrostatic interactions, hydrophobic interactions, etc., thus achieving the thickening and shear functions of well completion fluids (Ajieh et al., 2023; Akpan, 2024; Chu and Lin, 2019; Gautam et al., 2024). According to the source, viscosities can be divided into natural and modified polymers, as well as synthetic polymers. Natural and modified polymers, such as xanthan gum, cellulose, guar gum, etc., have the advantages of low cost and environmental friendliness, and are commonly used in conventional shallow well completion. However, in the high-temperature environment of deep and ultra-deep wells, ether bond breakage and ester bond hydrolysis in natural and modified polymer molecular chains can lead to the failure of completion fluids performance and even cause complex accidents such as blowouts (Allahvirdizadeh et al., 2016; Boul et al., 2016). Synthetic polymer viscosifiers, represented by polyacrylamide and its derivatives, can achieve excellent high-temperature stability by adjusting the type of functional groups, molecular structure, and molecular weight distribution (Caulfield et al., 2002; Sabhapondit et al., 2003). However, the current synthetic polymer molecular chains are prone to curling and even precipitation in high-temperature and high-density inorganic salts (such as calcium chloride, calcium bromide, etc.) well-completion fluids, leading to ineffective viscosity-enhancing effects (Sun et al., 2020). Therefore, it is urgent to improve the high temperature and high salt resistance of the viscosifiers.

At present, researchers mainly improve the comprehensive performance of polymers in terms of high temperature resistance and high salt resistance from the following aspects. First, the introducing rigid heterocycles (such as benzene rings, pyridine rings, five or six membered rings, etc.) to enhance the cohesion of polymer molecular chains, which limits the twisting and deformation of the chains, thus improving the temperature and salt resistance of the polymer (Chang et al., 2019; Li et al., 2025). For example, a copolymer based on pyridine monomers still exhibited certain thickening properties after aging for 16 h at 150 °C in 20% calcium chloride (Cao et al., 2017). Second, zwitterionic monomer with “anti-polyelectrolyte effect” can form antistatic shielding effect in saline environment, enabling polymer molecular chains to have excellent anti-curling ability in such conditions. For instance, a zwitterionic polymer FPOD showed an apparent viscosity of 37 mPa·s in calcium bromide brine and could tolerate high temperatures up to 150 °C (Wang et al., 2024). Third, through chemical or physical cross-linking, the polymer forms a tighter network structure, limiting the movement of polymer chains and thereby reducing the influence of temperature and salt ions on the conformation of polymer chains. Li et al. (2022b) synthesized a micro-crosslinked copolymer DADC for saturated sodium chloride drilling fluids, which retained an apparent viscosity of 25 mPa·s after aging at 200 °C for 16 h, but the polymer’s anti-calcium ion performance was not evaluated. Although progress has been made in the temperature and salt resistance of synthetic polymers, polymer viscosifiers for well completion fluids still face challenges such as poor temperature resistance and viscosity retention in high-temperature (≥180 °C), high-density (≥1.75 g/cm$^3$), and high-valence salt (calcium bromide) environments. Therefore, further research is needed on how to improve the comprehensive performance of polymers in high temperature and high-valence salt resistance through precise molecular structure design.

Herein, we developed a micro-crosslinked amphiphilic copolymer (i.e., A-DDAS), which demonstrated outstanding performance in enhancing viscosity and improving dynamic shear force within high-temperature and high-density calcium bromide brine. Specifically, the viscosifier was synthesized via free radical polymerization of N,N-dimethylacrylamide (DMAA), diallyl dimethyl ammonium chloride solution (DMDAAC), 2-acrylamido-2-methylpropanesulfonic acid (AMPS), [2-(methacryloyloxy) ethyl] dimethyl-(3-sulfopropyl) ammonium hydroxide (SBMA), and pentaerythritol triallyl ether crosslinking agent (APE). The micro-crosslinked structure significantly restricted the internal rotation of the polymer chain, facilitating the conformational transition of the molecular chain to an ordered state. Meanwhile, the electrostatic interaction between quaternary ammonium groups and sulfonic acid groups, along with the “internal salt bond” formed by SBMA, gradually dissociated as the salt ion concentration increased, increasing the swelling and solubility of polymer chains in brine. Compared with common viscosifiers (HE300 and Dristemp), a high-density calcium bromide brine (1.75 g/cm$^3$) containing 1.0 wt% A-DDAS copolymer maintained an apparent viscosity of 71 mPa·s and a yield of 7 Pa after aging at 180 °C for 16 h. Thanks to its sophisticated design, A-DDAS copolymer exhibited excellent viscosity-increasing and shear-force-improving properties in high-temperature and high-density brine, rendering it a promising candidate for deep and ultra-deep well completion operations.

## 2. Materials and methods

### 2.1. Materials

N,N-dimethylacrylamide (DMAA, 98%), diallyl dimethyl ammonium chloride (DMDAAC, 60% aqueous solution), 2-acrylamido-2-methylpropane sulfonic acid (AMPS, 98%), and [2-(methacryloyloxy) ethyl] dimethyl-(3-sulfopropyl) ammonium hydroxide (SBMA, 97%) were supplied by Aladdin Reagent Company (Shanghai, China). Sodium hydroxide (NaOH), ammonium persulfate (APS), and sodium hydrogen sulfite ($NaHSO_3$) were purchased from Sinopharm Chemical Reagent Co., Ltd. Pentaerythritol triallyl ether (APE) were purchased from Qingdao Keshengtai Chemical Technology Co., Ltd. Calcium bromide was obtained from Jiangsu Runfeng Synthetic Technology Co., Ltd., and

deionized water was prepared in the laboratory. HE300 and Dristemp viscosifier were purchased from Chevron Phillips Co., Ltd.

### 2.2. Synthesis of micro-crosslinked amphiphilic copolymer A-DDAS

The viscosifier A-DDAS was synthesized through free radical polymerization in an aqueous solution. First, 24 g of DMAA, 6 g of AMPS, 6 g of DMDAAC, 3.6 g of SBMA, and 0.12 g of APE were added to a beaker containing 150 mL of deionized water and stirred thoroughly. Next, the pH of the solution was adjusted to 8 using NaOH solution, and the mixture was transferred to a 500 mL three-necked flask. The solution was heated to 60 °C and stirred vigorously for 30 min under a nitrogen atmosphere to remove oxygen. Subsequently, 0.05 g APS and 0.05 g $NaHSO_3$ were added to initiate the polymerization reaction, which proceeded for 5 h to yield a transparent, gel-like product. Finally, the product was dried in a blast oven at 80 °C for 24 h and ground to 140 mesh to obtain the target viscosifier, A-DDAS. The synthesis route of A-DDAS was depicted in Fig. 1.

### 2.3. Synthesis of micro-crosslinked copolymer A-DDA

The synthesis of A-DDA follows the same procedure as that of A-DDAS, however, the key distinction lies in the omission of the zwitterionic monomer (SBMA) during the synthesis process.

### 2.4. Preparation of completion fluids

660 g of calcium bromide was slowly added to 300 mL of deionized water at 25 °C and stirred at 6000 rpm for 20 min with a high-speed mixer, then cooled to ambient temperature. Experimental results demonstrated that the maximum density of the calcium bromide brine could be elevated to 1.75 g/cm$^3$. The pH value of calcium bromide brine was 6.7.

### 2.5. Characterization of A-DDAS

The $^1$H-NMR spectrum of A-DDAS was obtained using a 600 MHz (Bruker, Switzerland) nuclear magnetic resonance spectrometer with $D_2O$ as the solvent. The molecular structure of the polymer was investigated using an IRTracer-100 Fourier transform infrared spectrometer (Shimadzu, Japan). The Thermo SCIENTIFIC ESCALAB Xi+ (Thermo Fisher, USA) was used to determine molecular composition of A-DDAS, with a monochromatic Al target as the excitation source and a voltage of 15 kV. The thermogravimetric analyzer (TA Instruments, USA) was used to evaluate the stability of polymers, with the temperature increased from 40 to 800 °C at a heating rate of 10 °C/min. The X Pert3 X-ray diffractometer (PANalytical, Netherlands) was used to test the crystallinity of A-DDAS. The rheological properties of completion fluids, shear thinning, thixotropic ring experiment, yield strength and modulus changes were measured using HAKEE MARS (Thermo Scientific, Germany). Different concentrations of A-DDA and A-DDAS were added to deionized water and calcium bromide brine. The shear rate was increased from 0 to 1000 s$^{-1}$, and the change in viscosity with shear rate was observed. The thixotropy experiment was to increase the shear rate to a certain value and then decrease it to zero at the same rate (Larson and Wei, 2019). In this article, the shear rate was set to 1000 s$^{-1}$. The static yield stress of 1.75 g/cm$^3$ calcium bromide brine was recorded after the addition of different contents of A-DDAS copolymer. Furthermore, the modulus variation with angular velocity was observed as the angular velocity was slowly increased from 0.1 to 100 rad·s$^{-1}$ in these brine samples.

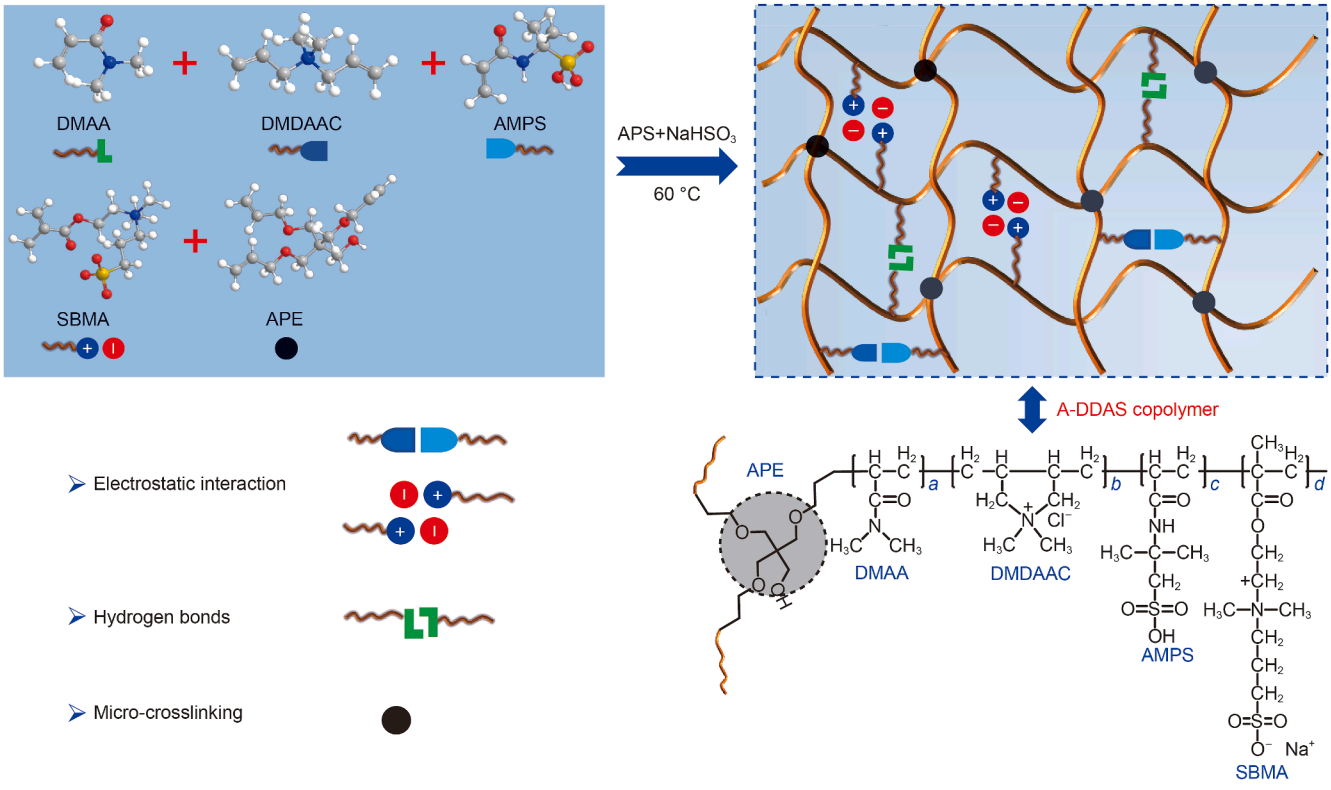


**Fig. 1.** Synthesis route of micro-crosslinked amphiphilic copolymer A-DDAS.

### 2.6. Performance of completion fluids

Different contents of copolymers were slowly added into calcium bromide brine. Calculating the apparent viscosity (AV), plastic viscosity (PV), and yield point (YP) of the completion fluids according to the formula:

$$AV = 0.5 \times \theta_{600}(\text{mPa·s}) \quad (1)$$

$$PV = \theta_{600} - \theta_{300}(\text{mPa·s}) \quad (2)$$

$$YP = 0.511 \times (\theta_{300} - PV)(\text{Pa}) \quad (3)$$

where $\theta_{600}$ and $\theta_{300}$ were dial readings at 600 and 300 rpm, respectively.

The calcium bromide brine with different A-DDAS contents was poured into the slurry cup of the six-speed viscometer. The rotational speed was set to 600 rpm and stirred for 10 s, followed by a 10-s rest period. The rotational speed was then switched to 3 rpm, and the reading on the six-speed viscometer was recorded at this point, which represents the initial gel strength.

The calcium bromide brine with different A-DDAS concentrations was poured into the slurry cup of the six-speed viscometer. The rotational speed was set to 600 rpm and stirred for 10 s, followed by a 10-min rest period. The rotational speed was then switched to 3 rpm, and the reading on the six-speed viscometer was recorded at this point, which represents the ultimate gel strength.

Three types of viscosifiers powders (A-DDAS, Dristemp and HE300) were prepared into a solution with a concentration of 300 mg/L using ultrapure water. A single colony was inoculated into a liquid culture medium and cultured in an air shaker. The optical density (OD) was measured to ensure the bacteria were in the logarithmic growth phase. NaCl solution (20 g/L) was used as a blank control, while the test sample served as a parallel control. The bacterial solution was diluted with NaCl solution, and its luminescence was measured with a single-tube multifunctional detector to confirm stability. After the addition of the bacterial solution, the 96-well plate was immediately transferred to a microplate luminescence detector (Berthold, Germany) and shaken at high speed to ensure thorough contact between the bacterial solution and the water sample. The plate was then exposed to air for 15 min. Following the exposure, the luminescence was measured again using a bioluminescence detector. Finally, the inhibition rate was calculated using the following formula:

$$E = [(I_0 - I)/I_0] \times 100\% \quad (4)$$

In the formula: $E$ was the luminescence inhibition rate; $I$ and $I_0$ represented the average luminescence values of the test sample and the blank control group, respectively, after 15 min of exposure. Dose-response curves were plotted using the sample concentration and the inhibition rate. The curve was then fitted, and the sample concentration corresponding to a 50% inhibition rate was determined as the $EC_{50}$.

The zeta potential values of calcium bromide brine with different A-DDAS contents, both before and after aging, were measured using a Zetasizer Nano Z (Malvern, UK) nanoparticle characterization system.

### 2.7. Mechanism analysis

Density functional theory calculations were employed to assess the water solubility of copolymers in calcium bromide brine of varying densities. Transmission electron microscopy (TEM) was utilized to visualize the molecular structures of 1.0 wt% A-DDA and A-DDAS in deionized water, 1.4 g/cm$^3$ calcium bromide brine, and 1.75 g/cm$^3$ calcium bromide brine.

## 3. Results and discussion

### 3.1. Characterization of the A-DDAS copolymer

In order to verify the successful preparation of A-DDAS copolymer, the molecular structure was characterized by $^1$H-NMR, FTIR and XPS. As depicted in Fig. 2(a), the chemical shifts of the two methyl hydrogen in DMAA appeared at approximately 2.9 ppm. The proton peaks of methyl (–$CH_3$) and methylene (–$CH_2$) groups in DMDAAC were observed at 3.0–3.2 ppm. The chemical shifts of the two methyl hydrogen (–$CH_3$) in AMPS were detected at 1.5 ppm. The peaks at 3.1 and 3.9 ppm corresponded to the –$CH_2$ group connected to the sulfonic acid group and the –$CH_2$ group connected to the erster bond in SBMA, respectively. As a result, the chemical shifts in the NMR spectra of each monomer indicated that the copolymer was successfully synthesized. In addition, FTIR was employed to further elucidate the molecular structure of the copolymer. As shown in Fig. 2(b), the peak at 2942 cm$^{-1}$ was attributed to the asymmetric stretching vibration of methyl and methylene in the copolymer. The peak at 1725 cm$^{-1}$ was derived from the stretching vibration of carbonyl (C=O) in SBMA. The peak at 1658 cm$^{-1}$ was attributed to the stretching vibration of amide group in DMAA. The peak at 1508 cm$^{-1}$ corresponded to the C–N/N–H stretching vibrations in AMPS. Additionally, the peak at 1214 and 1136 cm$^{-1}$ were the S=O stretching vibrations of the sulfonic acid group, further confirming the presence of AMPS. Moreover, it could be seen from Fig. 2(c) that the elements of all monomers exist, which further proven the occurrence of copolymerization. In particular, the split peak fitting results of C1*s* in Fig. 2(d) shown that the peak at 284.44 eV may corresponded to the C=O of the copolymer, and the peak at 284.80 eV was attributed to the C–C of the copolymer. Besides, the C1*s* peak at 285.95 eV corresponded to the C–S and C–N, and the C1*s* peak at 287.43 eV corresponded to the C–O–C, further validating the successful preparation of the target product.

The temperature of deep and ultra-deep oil and gas reservoirs is high, and the high-temperature resistance performance of viscosifier is the key to the stability of completion fluids (Reinoso et al., 2019). As depicted in Fig. 3(a), the thermal degradation of the A-DDAS copolymer occurred in four distinct stages as temperature increased. Specifically, in the first stage (40–158 °C), a 5% mass loss was observed, which could be attributed to the evaporation of free water and partial hydrolysis of amide groups in the copolymer. During the second stage (158–260 °C), an 8% mass loss was exhibited, resulting from the further hydrolysis of amide groups and the complete hydrolysis of the ester bonds derived from the SBMA monomer. The most significant degradation occurs in the third stage (260–473 °C), with a rapid 73% mass loss caused by the decomposition of sulfonic acid groups and cleavage of polymer side chains. Finally, as temperatures exceeded 473 °C, the copolymer underwent carbonization, ultimately yielding a residual mass of 9.5%. Usually, the crystallization of polymers had a crucial impact on their solubility properties. As depicted in Fig. 3(b), the diffraction pattern of the A-DDAS copolymer lack distinct peaks; instead, it exhibited typical diffuse peaks characteristic of amorphous polymers, suggesting that the molecular chains of the A-DDAS polymer were irregularly arranged.

### 3.2. Rheological performance of copolymer in deionized water

As is depicted in Fig. 4(a), with the increase of shear rate, the A-DDA and A-DDAS solutions with different contents exhibited good

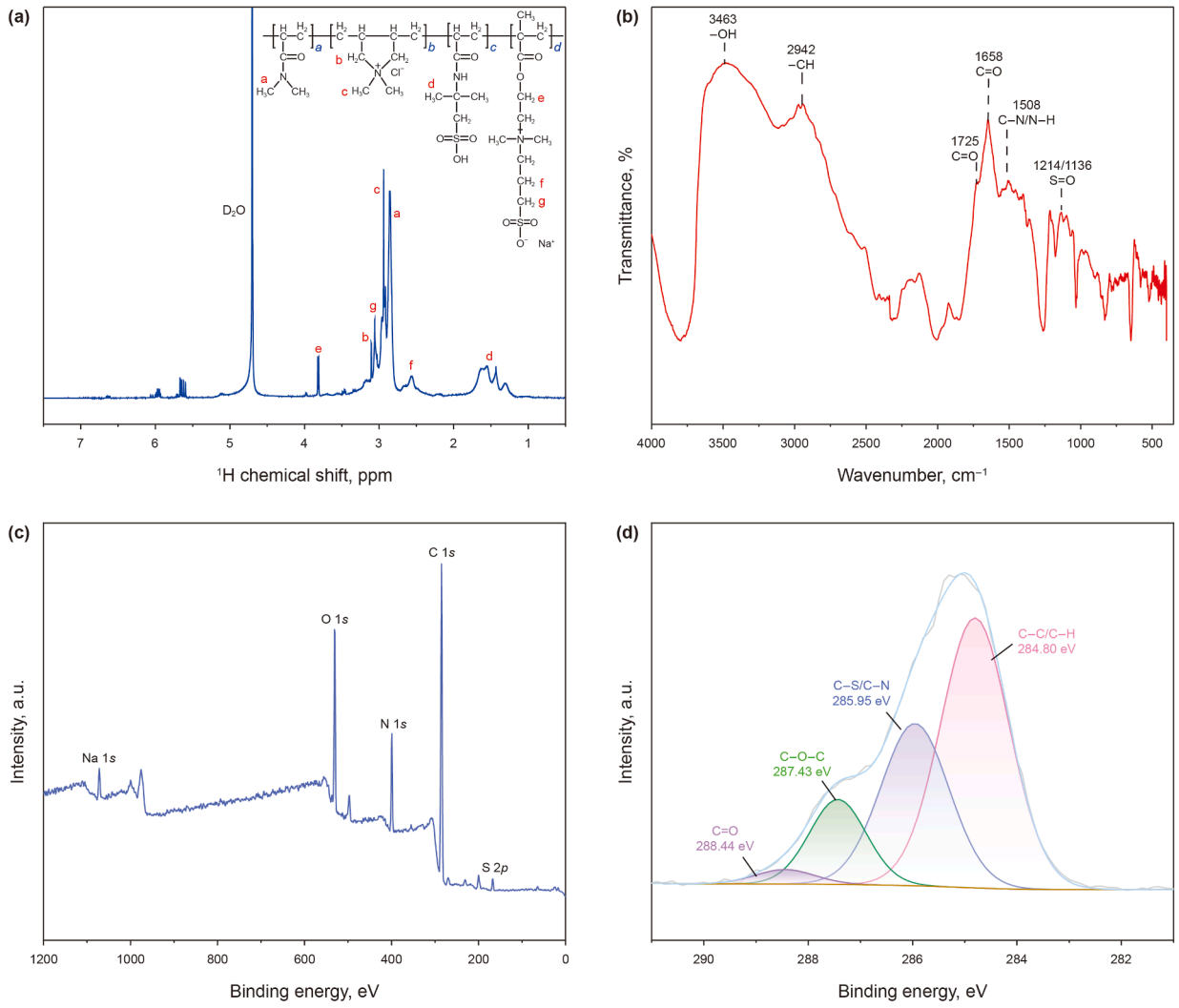


**Fig. 2.** **(a)** $^{1}$H-NMR curves of A-DDAS copolymer; **(b)** FTIR of A-DDAS copolymer; **(c)** Full XPS spectrum of the A-DDAS copolymer; **(d)** C-spectrum analysis of the A-DDAS copolymer.

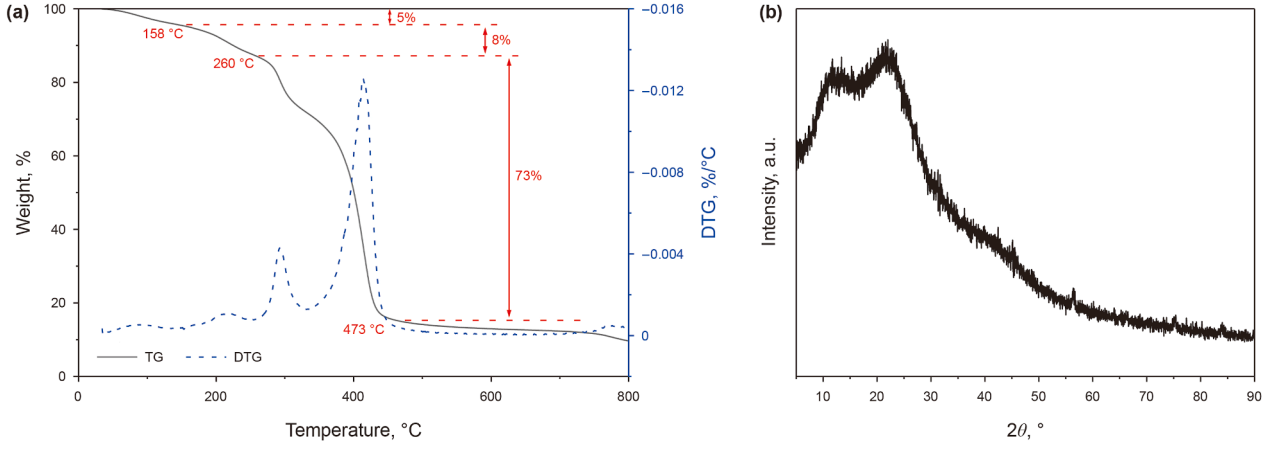


**Fig. 3.** **(a)** TGA curve of A-DDAS copolymer; **(b)** XRD curve of A-DDAS copolymer.

shear thinning behavior, but the viscosity of A-DDA solution was higher than that of A-DDAS solution. This was because in deionized water, A-DDAS polymer chain demonstrated a contracted conformation due to the action of internal salt bonds between zwitterionic groups. This conformation led to a significantly smaller hydrodynamic volume for A-DDAS relative to A-DDA,

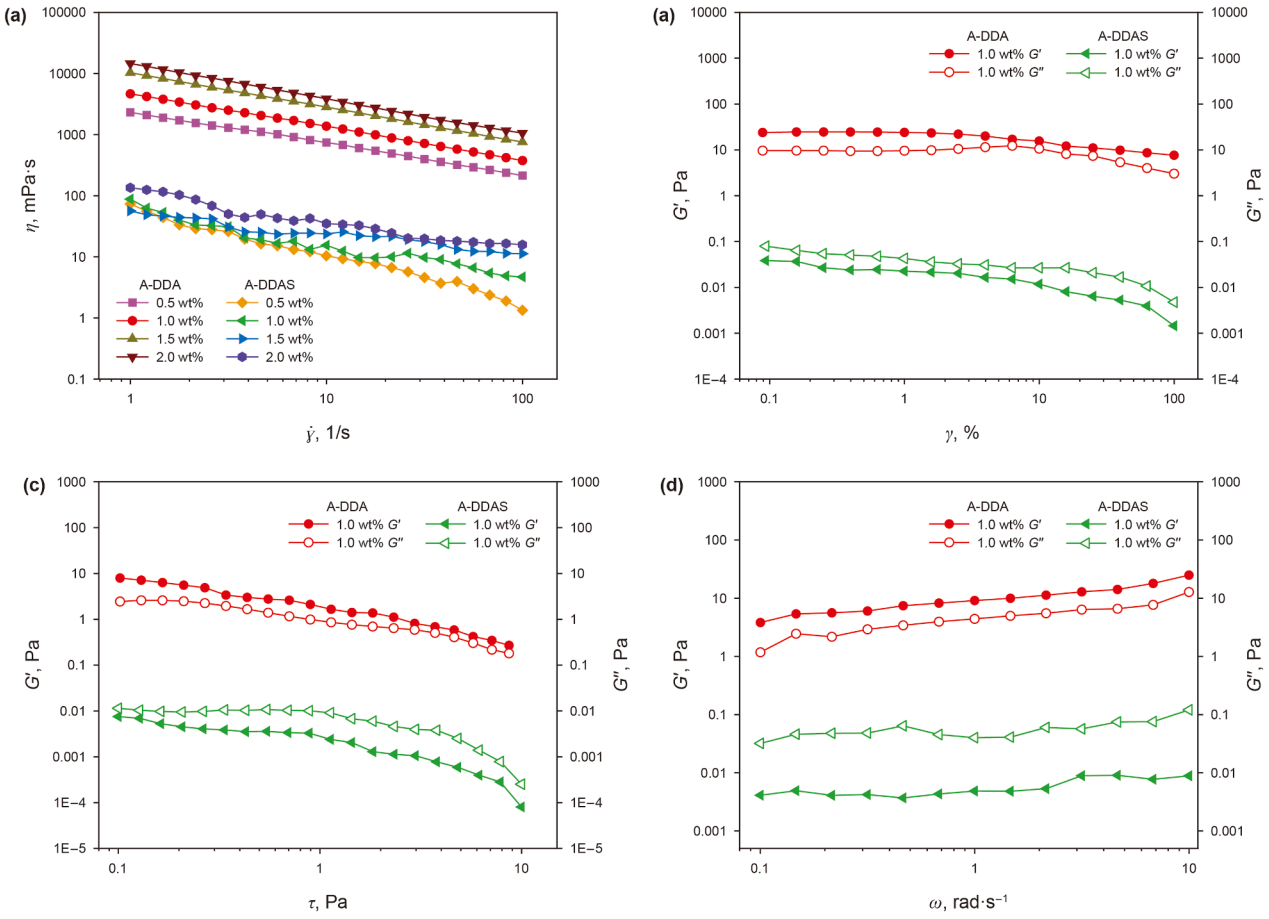


**Fig. 4.** Rheological performance of A-DDA and A-DDAS in deionized water. **(a)** Shear thinning curves; **(b)** Linear viscoelastic zone tests; **(c)** Stress scanning curves; **(d)** Frequency scanning curves.

thereby resulting in lower solution viscosity. Furthermore, through oscillation scanning experiments, it could be observed in Fig. 4(b) that within the linear viscoelastic region, the storage modulus $G'$ and loss modulus $G''$ of the 1.0 wt% A-DDA solution were both higher than those of the 1.0 wt% A-DDAS solution. It was worth noting that the elastic modulus $G'$ of A-DDA solution was higher than its loss modulus $G''$, indicating that the solution predominantly exhibited elastic properties. In contrast, for the A-DDAS solution, the elastic modulus $G'$ was lower than its loss modulus $G''$, suggesting that the solution was mainly viscous. In addition, as illustrated in Fig. 4(c) and (d), with the continuous increase of stress and scanning frequency, the storage modulus $G'$ and loss modulus $G''$ of A-DDA solution changed more rapidly compared to those of the A-DDAS solution. This was because due to the action of internal salt bonds, A-DDAS formed a strong network structure in aqueous solution, with a smaller hydrodynamic volume and the ability to resist higher external forces. Conversely, the relatively large hydrodynamic volume of the A-DDA solution caused its molecular chain conformation to change significantly under increasing shear forces, leading to substantial variations in modulus.

### 3.3. Rheological performance of copolymer in calcium bromide brine

As depicted in Fig. 5(a) and (b), 1.0 wt% of A-DDA and A-DDAS were added to calcium bromide brine of varying densities to investigate their shear thinning behavior. When the completion fluids were pumped into the wellbore through the drill pipe, the flow rate and the shear rate were high. If the completion fluids could maintain low viscosity at a high shear rate, it could reduce the pump pressure and reduce the power consumption in the water. On the other hand, low viscosity fluids could reduce the impact on the production layer, prevent loss of the formation due to excessive pressure fluctuations, and prevent sand production. The experimental results demonstrated that with the increase in the density of calcium bromide brine, the viscosity of the calcium bromide brine containing A-DDAS gradually escalated and manifested excellent shear thinning characteristics. Conversely, the viscosity of the calcium bromide brine containing A-DDA declined as the density of calcium bromide increased. This was because the increase in calcium bromide density induced A-DDA molecules to gradually curl and contract, whereas A-DDAS molecules tend to expand progressively. Maintaining low viscosity of drilling and completion fluids at high shear rates was beneficial for increasing drilling speed (Mohamed et al., 2021). In addition, calcium bromide brine containing 0.5, 1.0, 1.5 and 2.0 wt% of A-DDAS all exhibited outstanding shear-thinning behavior (Fig. 5(c)). Specifically, the brine with 2.0 wt% A-DDAS had a viscosity of 622 mPa·s at 0 $s^{-1}$, whereas at a shear rate of 1000 $s^{-1}$, its viscosity decreased to 71 mPa·s, representing 88.3% reduction.

Fig. 5(d) illustrated that, across four distinct A-DDAS concentrations, the loss modulus $G''$ of the calcium bromide brine consistently exceeded the storage modulus $G'$. This observation indicated that the calcium bromide brine formulated with A-DDAS exhibited predominantly viscous behavior. As the A-DDAS

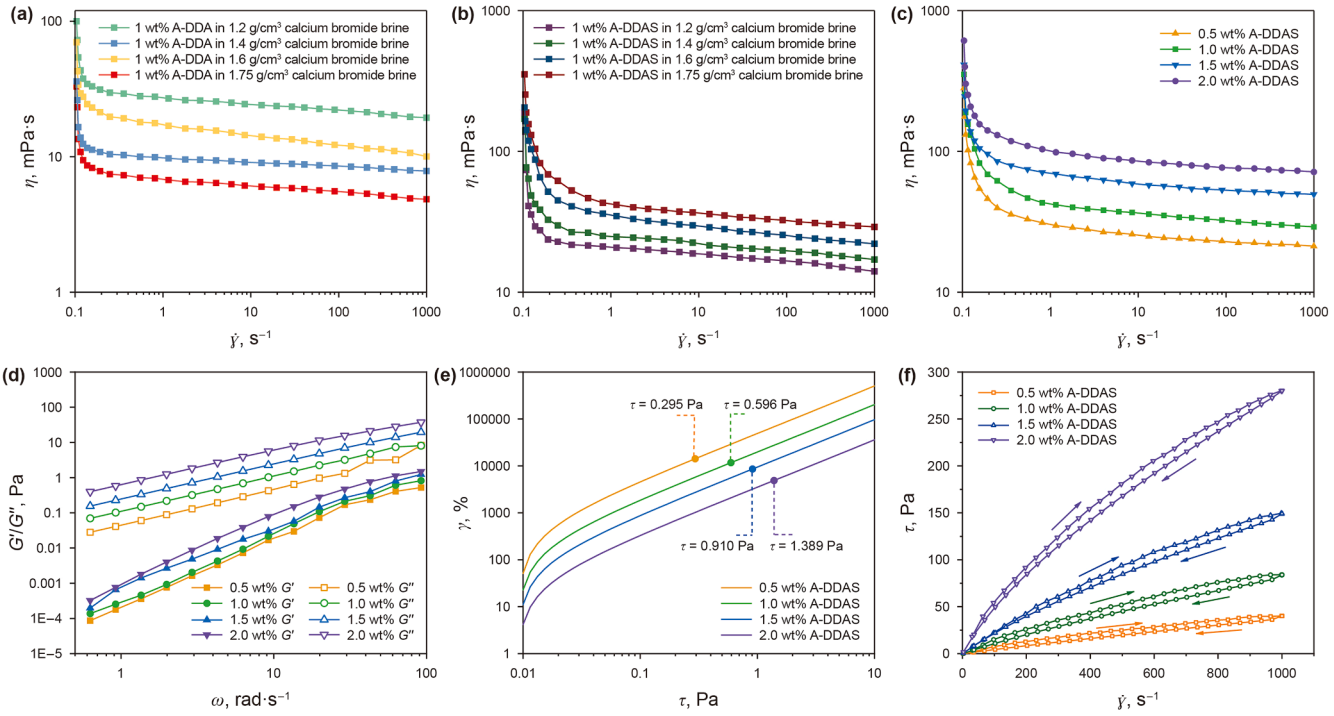


**Fig. 5.** **(a)** Shear thinning curves of 1.0 wt% A-DDA in different density calcium bromide brine; **(b)** Shear thinning curves of 1.0 wt% A-DDAS in different density calcium bromide brine; **(c)** Shear thinning curves of different A-DDAS in 1.75 g/cm$^3$ calcium bromide brine; **(d)** Modulus of different A-DDAS in 1.75 g/cm$^3$ calcium bromide brine; **(e)** Yield stress curves of different A-DDAS in 1.75 g/cm$^3$ calcium bromide brine; **(f)** Thixotropic loop curves of different A-DDAS in 1.75 g/cm$^3$ calcium bromide brine.

concentration increased, both the storage modulus $G'$ and loss modulus $G''$ of the calcium bromide brine demonstrated an upward trend. Notably, when the A-DDAS content reached 1.5 and 2.0 wt%, the disparity between the loss modulus $G''$ and the storage modulus $G'$ remained nearly constant, suggesting that a stable network structure had been established within the calcium bromide brine. The characteristic of plastic fluid is that the solution will only flow when the shear stress applied to the solution exceeds a certain value (Jeong, 2019). Fig. 5(e) depicted the evolution of static yield stress as a function of increasing shear stress in 1.75 g/cm$^3$ calcium bromide brine formulations with varying A-DDAS concentrations. As the concentration of the A-DDAS copolymer risen, the entanglement and reinforcement of polymer chains lead to the formation of a stable network structure within the calcium bromide brine. This structural development significantly elevated the yield stress required to initiate flow in the initially quiescent calcium bromide brine. Specifically, when the A-DDAS content in the calcium bromide brine increased incrementally from 0.5 to 2.0 wt%, the corresponding yield stress of the brine escalated from 0.295 to 1.389 Pa, demonstrating a pronounced concentration-dependent enhancement.

Good thixotropy can enhance the pumping performance of completion fluids (Larson and Wei, 2019). Thixotropy loop testing assesses the thixotropic strength of calcium bromide brine by measuring shear stress fluctuations during shear rate ramp-up and ramp-down cycles, which generate hysteresis loops (Skadsem et al., 2019). As illustrated in Fig. 5(f), across the four A-DDAS concentrations tested, the ascending curves of the brine consistently exceeded the descending curves. This phenomenon could be attributed to the distinct structural states of the brine during different phases of the testing cycle. During the ramp-up stage, as the shear rate increased from low to high, the internal structure of the brine remained intact, necessitating a higher shear stress to initiate and sustain the flow of the calcium bromide brine. Conversely, during the ramp-down stage, the brine's structure had been disrupted and had not fully recovered, resulting in a lower shear stress requirement for maintaining flow compared to the ramp-up stage. With the increment of A-DDAS concentration, the shear stress needed to maintain the flow of calcium bromide brine increased in both the ramp-up and ramp-down stages, and the area of the hysteresis loop expanded correspondingly. This observation indicated that an increase in A-DDAS concentration significantly enhanced the thixotropy of calcium bromide brine.

### 3.4. Performance of A-DDAS in high-temperature calcium bromide brine

As we know, solid-free completion fluids should exhibit favorable rheological properties (viscosity, shear force) in the high-temperature environments of deep and ultra-deep wells to prevent sand settling, pipe jamming, or blockage of perforation holes (You et al., 2024). Additionally, by adjusting the dosage of inorganic salts, the density of completion fluids can be regulated to prevent formation collapse or fluid influx (such as gas and water invasion), thereby ensuring wellbore safety. Therefore, viscosifier play a crucial role in the rheological properties of inorganic salt completion fluids with different densities at high temperatures. As discussed above, the viscosity of A-DDA gradually decreased with increasing salt concentration, whereas A-DDAS exhibited the opposite trend due to the anti-polyelectrolyte effect. Therefore, this study focused solely on exploring the performance of A-DDAS in high-temperature, high-density calcium bromide brine. As shown in Fig. 6(a–c), in a 1.75 g/cm$^3$ calcium bromide brine, as the concentration of A-DDAS copolymer increased from 0.2 to 1.0 wt%, the AV, PV, and YP of the brine increased from 16.5 mPa·s, 15 mPa·s, and 1.5 Pa to 79 mPa·s, 68 mPa·s, and 11 Pa, respectively. Notably, when the polymer concentration reached 1.0 wt%, the viscosity and shear force of the calcium bromide brine showed a significant

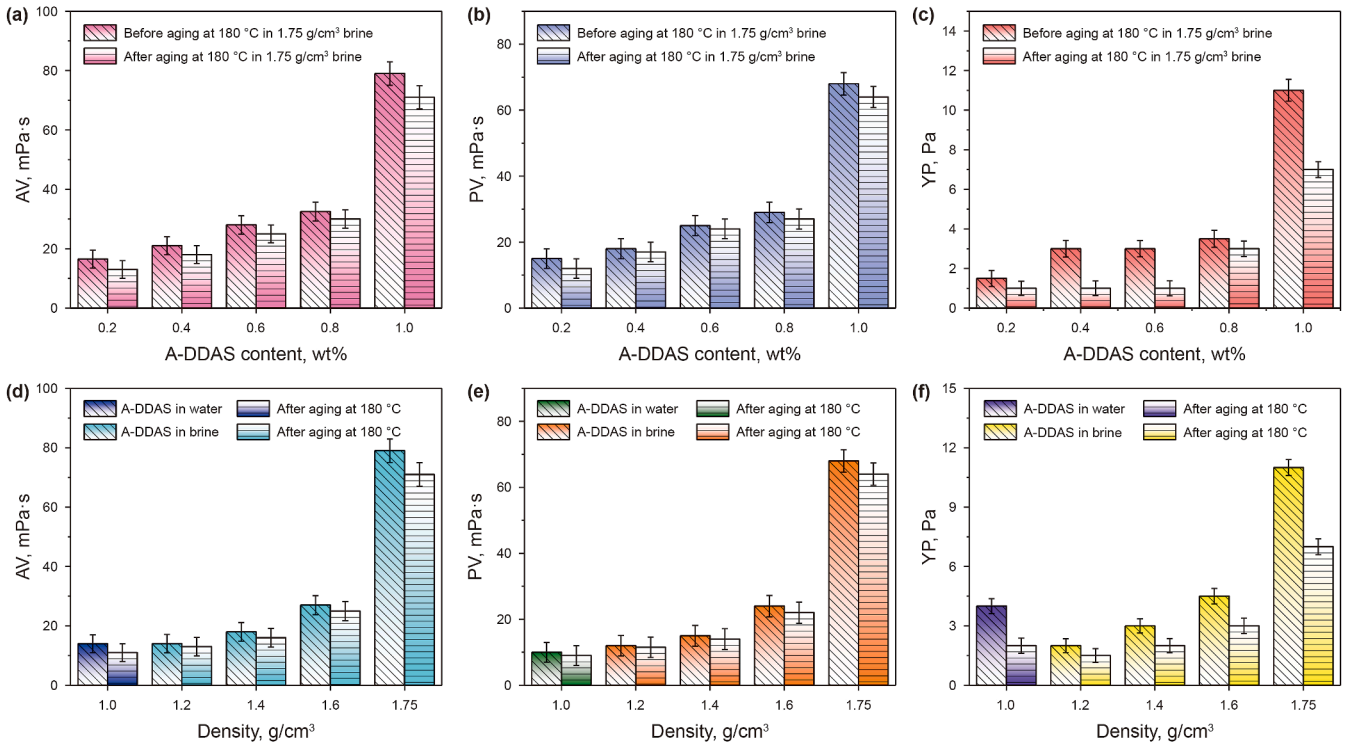


**Fig. 6.** Rheological properties of calcium bromide brine containing A-DDAS copolymer before and after aging: **(a)** and **(d)** AV; **(b)** and **(e)** PV; **(c)** and **(f)** YP.

increase, consistent with previously reported results (Wang et al., 2024). This phenomenon may be attributed to the fact that when the A-DDAS concentration exceeded the critical entanglement concentration (C*) of the polymer chains, the polymer chains began to entangle with each other, forming a "network structure" that significantly increased the brine viscosity. In addition, after aging at 180 °C for 16 h, the viscosity and yield point of the calcium bromide brine containing polymer demonstrated a decreasing trend. Specifically, the AV, PV, and YP of calcium bromide brine containing 1.0 wt% A-DDAS were 71 mPa·s, 64 mPa·s, and 7 Pa, respectively, still maintaining high viscosity and yield point after high-temperature aging. Usually, the density of completion fluids needed to be adjusted according to different geological conditions and engineering requirements. Therefore, the performance of the A-DDAS copolymer in calcium bromide brine of varying densities was investigated. As shown in Fig. 6(d–f), at a fixed A-DDAS content of 1.0 wt%, as the density of the calcium bromide brine increased from 1.2 to 1.75 g/cm$^3$, the AV increased from 14 to 79 mPa·s, the PV increased from 10 to 68 mPa·s, and the YP increased from 4 to 11 Pa. This can be attributed to two factors: First, as the salt concentration increased, the degree of dissociation of internal salt bonds in the A-DDAS copolymer increased, leading to an expansion of the hydrodynamic volume and an increase in viscosity. Second, salt ions attracted free water molecules to form a hydration layer, which promoted the entanglement of polymer molecular chains to some extent, resulting in increased flow resistance and viscosity. Therefore, the A-DDAS copolymer demonstrated excellent viscosity and shear force enhancement properties in high-temperature, high-density calcium bromide brine.

To further evaluate the performance of A-DDAS, it was compared with two commonly used viscosifiers for solid-free completion fluids, HE300 and Dristemp. The viscosifier 80A51 exhibited poor solubility in high-density calcium bromide brine and was highly prone to precipitation, making it impossible to accurately determine its performance. Therefore, 80A51 was not included for comparison in this study. As illustrated in Fig. 7(a–c), the rheological parameters of 1.0 wt% HE300, Dristemp, and A-DDAS were measured before and after aging in a 1.75 g/cm$^3$ calcium bromide brine. The results clearly showed that the AV, PV, and YP of the calcium bromide brine containing A-DDAS were significantly higher than those of the brine with HE300 and Dristemp. Specifically, after aging at 180 °C for 16 h, the yield point of the brine with A-DDAS reached 7 Pa, which was considerably higher than that of HE300 (2 Pa) and Dristemp (1 Pa). In summary, the above experiments demonstrated that A-DDAS had strong temperature resistance and viscosity increasing ability, and was expected to be applied in deep and ultra-deep complex formation completion operations.

In order to measure the suspension ability of the completion fluids on the solid phase in a static state, we measured the initial and ultimate gel strength of the calcium bromide brine, and the results are shown in Fig. 8. From Fig. 8(a) and (b), it can be seen that as the polymer content increased, the initial and ultimate gel strength of the calcium bromide brine also increased. When the content of A-DDAS reached 1.0 wt%, the initial gel strength of the calcium bromide brine was 6 Pa and the ultimate gel strength was 7 Pa. After 16 h of hot rolling aging at 180 °C, the initial gel strength of the calcium bromide brine was 4 Pa and the final shear force was 5 Pa, indicating that the calcium bromide brine still had good suspension performance for solid particles. This article changed the content of A-DDAS and measured the zeta potential of calcium bromide brine at different contents, as shown in Fig. 8(c). From Fig. 8(c), it can be seen that both before and after aging, the zeta potential of the calcium bromide brine with A-DDAS added was negative. When the content of A-DDAS increased to 1.0 wt%, the zeta potential of the calcium bromide brine was −4.12 mV. After 16 h of hot rolling aging at 180 °C, its zeta potential was −3.62 mV.

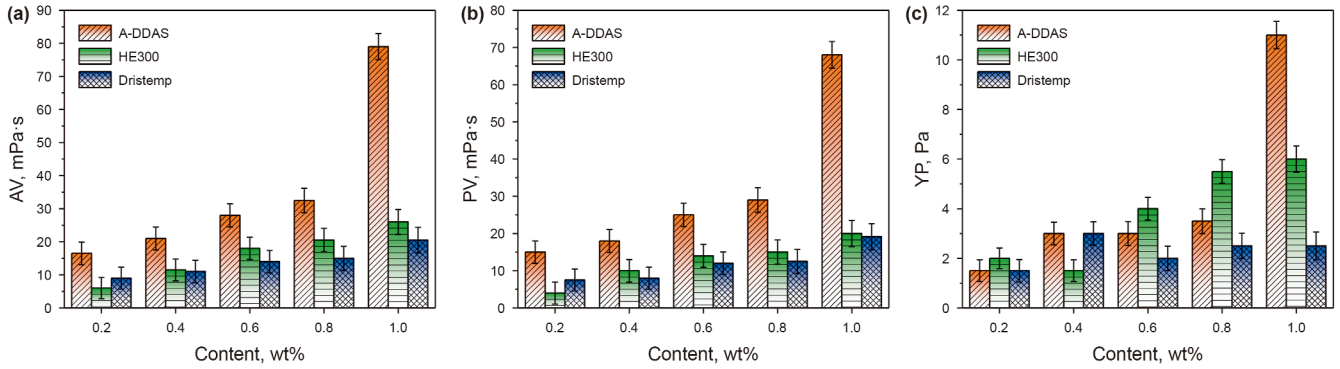


**Fig. 7.** Rheological properties of 1.75 g/cm$^3$ calcium bromide brine containing 1.0 wt% different viscosifier before and after aging: **(a)** AV; **(b)** PV; **(c)** YP.

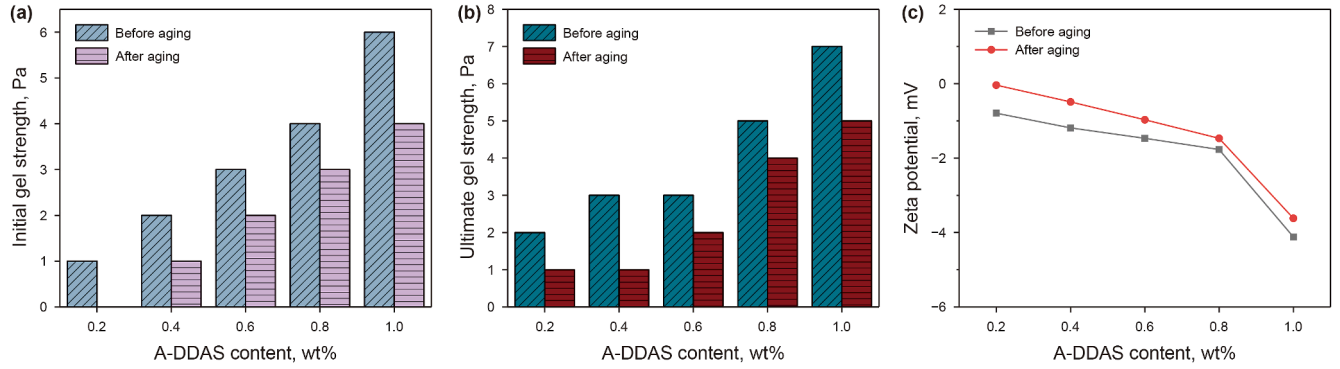


**Fig. 8.** Initial and ultimate gel strength, zeta potential of A-DDAS with different contents before and after aging in 1.75 g/cm$^3$ calcium bromide brine: **(a)** Initial gel strength; **(b)** ultimate gel strength; **(c)** zeta potential.

This indicated that as the content of A-DDAS increased, the degree of polymer extension in the calcium bromide brine gradually increased, and the stability of the completion fluids gradually improved.

In order to measure the toxicity of the viscosifier A-DDAS, we conducted biotoxicity experiments and measured the inhibition rates and $EC_{50}$ values of A-DDAS, Dristemp, and HE300 against *Vibrio fischeri*. The results are shown in Fig. 9(a–c). From Fig. 9(a–c), it can be seen that when the concentration reaches 150 mg/L, Dristemp has the highest inhibition rate of 46.12% against *Vibrio fischeri*, while the inhibition rates of A-DDAS and HE300 were 23.06% and 28.07%, respectively. By calculating the inhibition rates, the $EC_{50}$ values of A-DDAS, Dristemp, and HE300 were 474.62, 162.85, 326.93, indicating that A-DDAS has lower toxicity compared to Dristemp and HE300.

### 3.5. Microstructure of copolymers in deionized water and calcium bromide brine

The spatial distribution morphology (i.e. conformation) of polymer chains in solution is the core determinant of their macroscopic properties (Harding et al., 2011). To investigate this relationship, the solubility and micro-structural characteristics of 1.0 wt% A-DDA and A-DDAS copolymers were examined in deionized water and calcium bromide brine of varying densities. As shown in Fig. 10(a), the deionized water solution of A-DDA copolymer exhibited a clear state, and transmission electron microscopy (TEM) also indicated that it was fully dissolved. In contrast, the A-DDAS copolymer solution exhibited turbidity and contained undissolved particulate matter (Fig. 10(d)), indicating limited solubility under these conditions. However, when added to

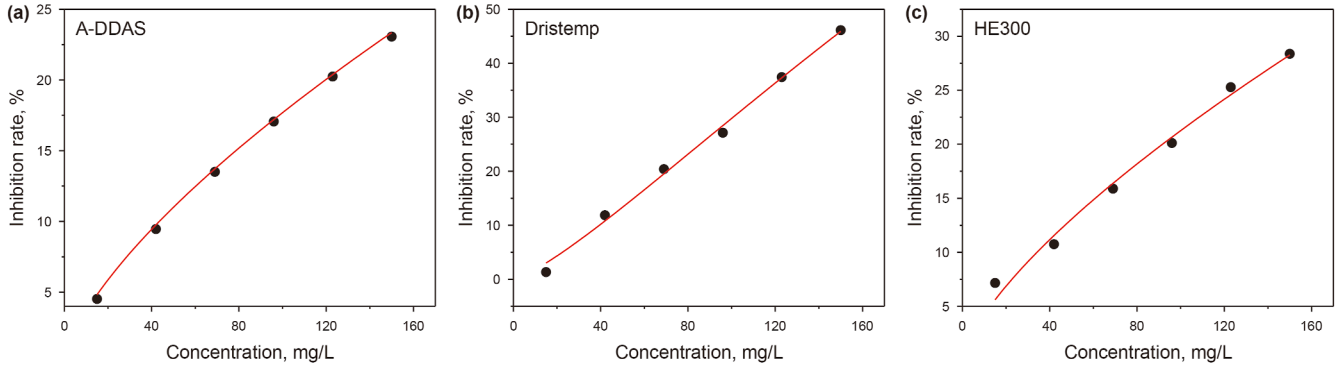


**Fig. 9.** The inhibition rates of viscosifiers on *Vibrio fischeri* varies with concentration curves: **(a)** A-DDAS; **(b)** Dristemp; **(c)** HE300.

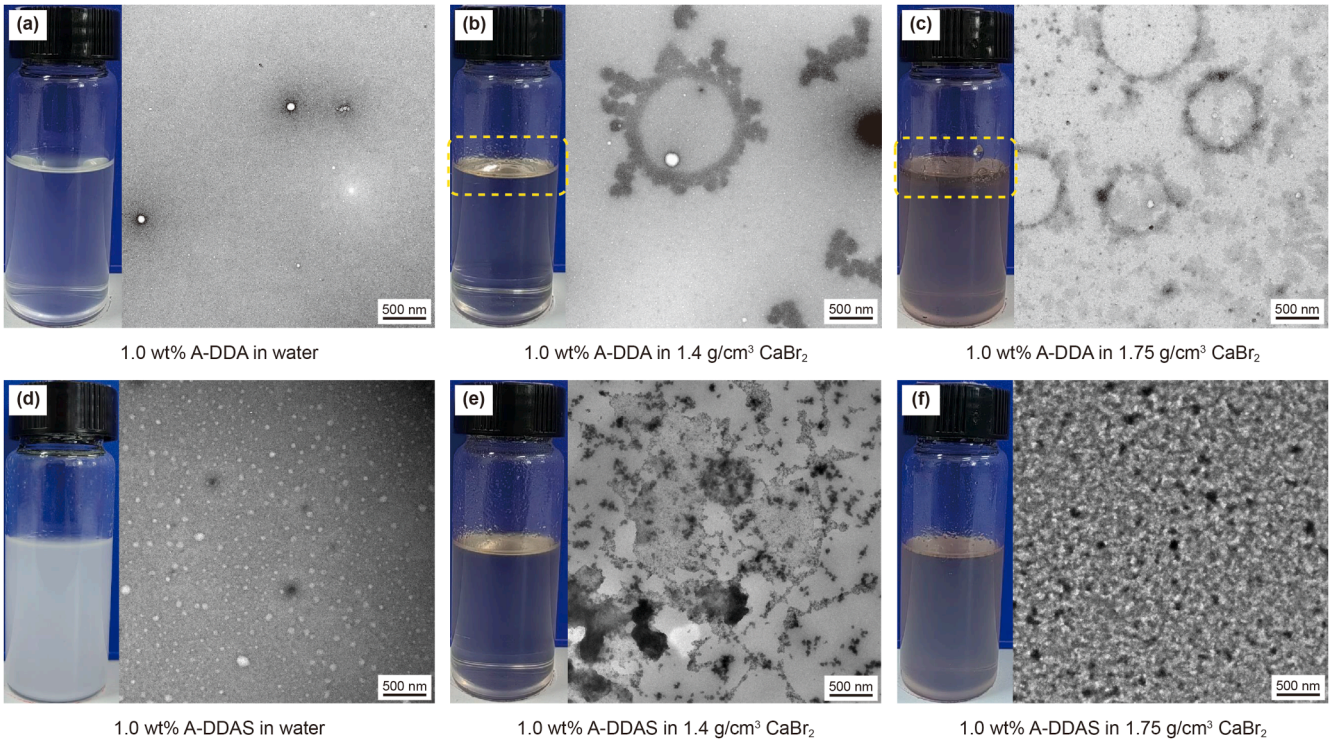


**Fig. 10.** Transmission electron microscopy image of water and calcium bromide brine. **(a)** 1.0 wt% A-DDA in deionized water; **(b)** 1.0 wt% A-DDA in 1.4 g/cm$^3$ calcium bromide brine; **(c)** 1.0 wt% A-DDA in 1.75 g/cm$^3$ calcium bromide brine; **(d)** 1.0 wt% A-DDAS in deionized water; **(e)** 1.0 wt% A-DDAS in 1.4 g/cm$^3$ calcium bromide brine; **(f)** 1.0 wt% A-DDAS in 1.75 g/cm$^3$ calcium bromide brine.

a 1.4 g/cm$^3$ calcium bromide brine, the A-DDA copolymer chains began to curl and precipitate (Fig. 10(b)). This behavior intensified at a higher density of 1.75 g/cm$^3$, where visible precipitates accumulated at the brine's surface, and TEM analysis revealed insoluble aggregates (Fig. 10(c)). Conversely, when the same mass of A-DDAS copolymer was added to a 1.4 g/cm$^3$ calcium bromide brine, the solubility of the copolymer began to increase due to the gradual opening of some ionic bonds in the polymer molecular chains (Fig. 10(e)). Specifically, A-DDAS copolymer did not precipitate like A-DDA copolymer in a 1.75 g/cm$^3$ calcium bromide brine, and transmission electron microscopy also demonstrated its excellent solubility in calcium bromide brine (Fig. 10(f)). These observations indicated that electrostatic interactions restrict the solubility of A-DDAS in deionized water, resulting in a compact molecular conformation and reduced hydrodynamic volume (Xie et al., 2018). In calcium bromide brine, however, the anti-polyelectrolyte effect promoted dissociation of "internal salt bonds", expanding the molecular structure and enhancing both solubility and viscosity (Xiao et al., 2018).

### 3.6. Molecular simulation and density functional theory

The spatial distribution of polymer molecular chains in calcium bromide brine was related to the electrostatic interactions between the constituent monomers and ions. The electrostatic potential (ESP) plot (Fig. 11(a)) illustrated the charge distribution of DMAA, DMDAAC, AMPS, and SBMA molecules. It could be seen that positive charges were concentrated on the nitrogen atom of the positively charged group, while negative charges were mainly distributed on multiple oxygen atoms of the negatively charged group. Notably, the SBMA exhibited a higher absolute charge density compared to other monomers.

To further investigate these interactions, molecular models of A-DDA and A-DDAS were constructed using Materials Studio in deionized water and 1.75 g/cm$^3$ calcium bromide brine. For deionized systems, a periodic box (40 nm × 40 nm × 40 nm) containing 1000 water molecules and one polymer chain was simulated. For calcium bromide brine systems, the periodic box included 1000 water molecules, 240 Ca ions and 480 Br ions. The binding energies of copolymer A-DDA and copolymer A-DDAS with water were calculated using Gaussian in both deionized water and 1.75 g/cm$^3$ calcium bromide brine. The results were presented in Fig. 11, and the binding energy calculation formulas were as follows:

$$E_B = E_{total} - E_1 - E_2 \quad (5)$$

Among them, $E_B$ represented the binding energy, $E_{total}$ was the total energy of the system, $E_1$ was the energy of the polymer in the box, and $E_2$ was the energy of the water in the box.

As illustrated in Fig. 11(d), in deionized water, the binding energy of A-DDA with water was −7.08 eV, while that of A-DDAS with water was −6.02 eV. This indicated that the solubility of A-DDA in water was superior to that of A-DDAS. The reason lies in that the introduction of the zwitterionic monomer SBMA in A-DDAS causes the polymer molecular chain of A-DDAS to contract, resulting in extensive aggregation among different molecules and consequently reducing its solubility in water. In the 1.75 g/cm$^3$ calcium bromide brine, the binding energy between A-DDA and water molecules was −5.45 eV, and the binding energy between A-DDAS and water molecules reached −9.42 eV. This was attributed to the fact that the influx of a large number of calcium ions weakens the electrostatic attraction between the positive and negative charge groups on the A-DDAS molecular chain. As a result, the molecular chain stretched, the aggregation phenomenon between molecules

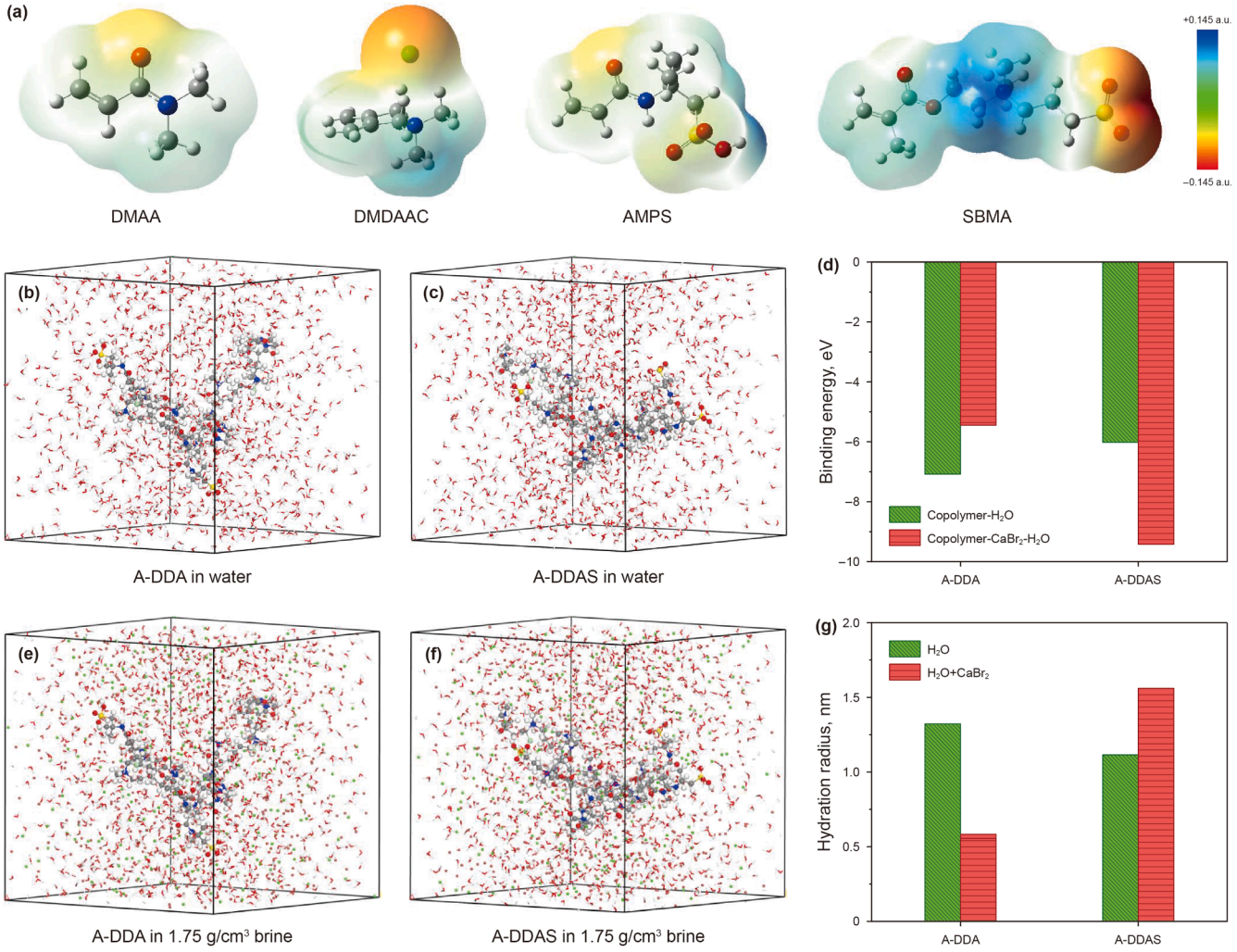


**Fig. 11.** **(a)** The electrostatic potential of four monomers; **(b)** and **(c)** Molecular models of A-DDA and A-DDAS in deionized water; **(e)** and **(f)** Molecular models of A-DDA and A-DDAS in 1.75 g/cm$^3$ calcium bromide brine; **(d)** Binding enengy of A-DDA and A-DDAS in deionized water; **(g)** Hydration radius of A-DDA and A-DDAS in 1.75 g/cm$^3$ calcium bromide brine and deionized water.

disappeared, and more hydrophilic groups could fully interact with water. Therefore, the solubility of A-DDAS in 1.75 g/cm$^3$ calcium bromide brine was significantly enhanced.

Hydraulic radius was an important indicator for measuring the performance of polymer viscosifiers, which could reflect the size of the space occupied by polymer molecules in solution and their dynamic volume. This article used molecular dynamics to measure the hydraulic radius of A-DDA and A-DDAS, using the following formula:

$$g_{\alpha\beta}(r) = \frac{v_s}{N_\alpha N_\beta} \sum_{i=1}^{N_\alpha} \frac{n_{i\beta}(r)}{4\pi r^2 \Delta r} \tag{6}$$

In the formula, $N_\alpha$ and $N_\beta$ were the particle numbers of $\alpha$ and $\beta$ respectively, $v_s$ was the volume of the box, and $n_{i\beta}(r)$ was the number of particles of type $b$ within a distance range from $r$ to $r + \Delta r$ from particle $i$.

From Fig. 11(g), it can be seen that the hydraulic radius of A-DDA and A-DDAS in water were 1.322 and 1.115 nm, respectively, indicating that A-DDA had stronger thickening performance in water than A-DDAS. However, in a calcium bromide brine with a density of 1.75 g/cm$^3$, the hydraulic radius of A-DDA decreased to 0.583 nm, indicating that as the concentration of calcium bromide increased, A-DDA produced a large amount of precipitation and the thickening effect sharply decreased. The increase in calcium ion concentration continuously opened the internal salt bonds in A-DDAS molecules, causing the molecular chains to gradually stretch and the hydraulic radius to rise to 1.560 nm, much higher than A-DDA. This once again proved that A-DDAS was a salt responsive polymer with excellent thickening properties in high-density calcium bromide brine.

### 3.7. Mechanism of A-DDAS copolymer response in calcium bromide brine

Through the above experiments and theoretical analysis, it was found that the thickening effect of A-DDAS copolymer was significantly altered in deionized water, low-density, and high-density calcium bromide brine. Therefore, as illustrated in Fig. 12, the salt response mechanism of A-DDAS copolymer was analyzed.

In deionized water, the electrostatic interaction between the quaternary ammonium groups in DMDAAC and the sulfonic acid groups in AMPS, coupled with the “internal salt bonds” within SBMA, induced a contracted conformation of the polymer

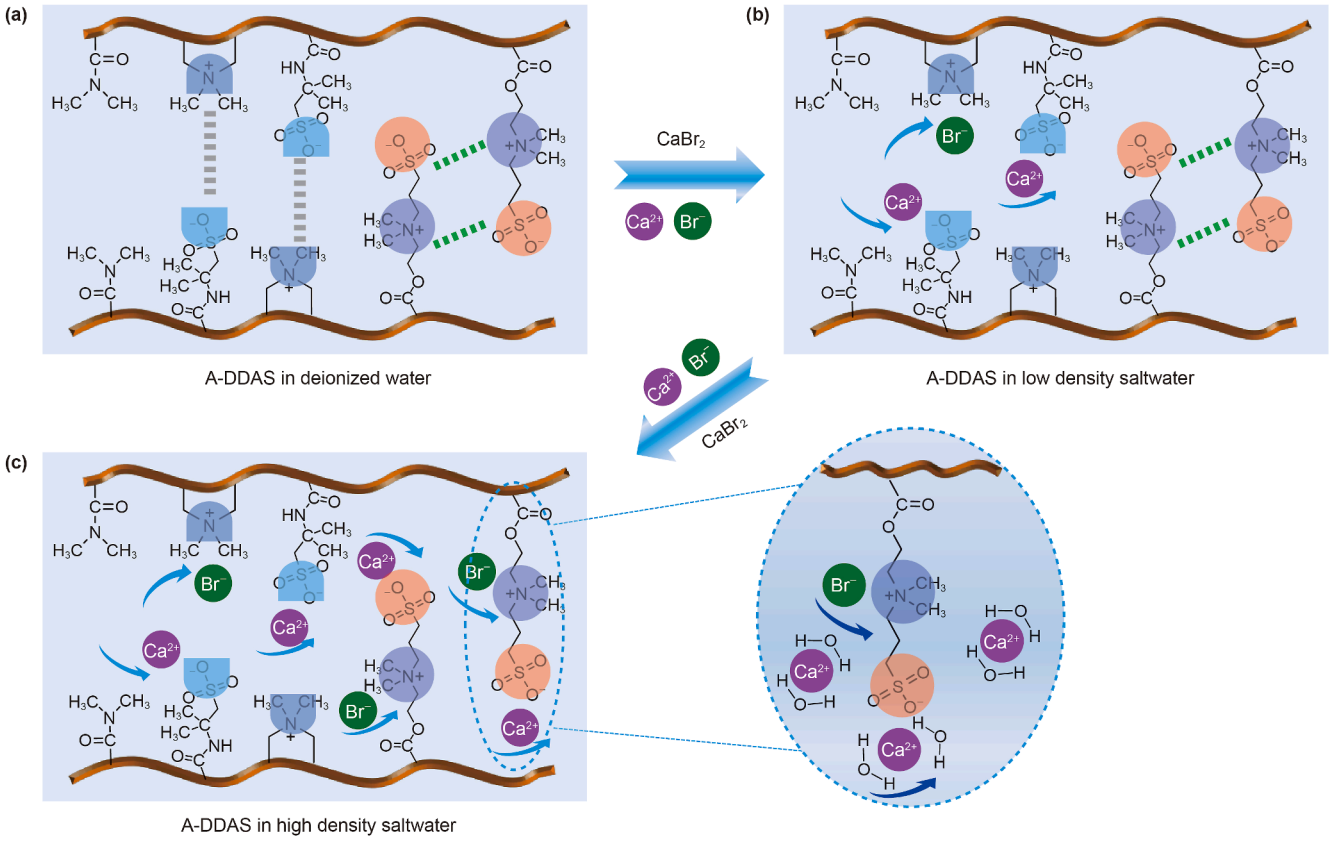


**Fig. 12.** Mechanism of A-DDAS copolymer response in calcium bromide brine.

molecular chains. Meanwhile, due to the binding effect of covalent micro-crosslinking structures, the free stretching and contraction motion between polymer molecular chains was significantly restricted. Consequently, under the combined influence of covalent micro-crosslinking and non-covalent electrostatic interactions, the molecular chains of A-DDAS copolymer were difficult to fully stretch, resulting in low hydrodynamic volume and poor solubility.

In low-density calcium bromide brine, a small amount of calcium and bromide ions infiltrated between the polymer molecular chains, shielding the electrostatic interactions between quaternary ammonium and sulfonic acid groups, which improved the stretching of the polymer chains and increased the swelling degree of A-DDAS to some extent. However, despite partial expansion of the polymer chain, the "internal salt bonds" in the polymer chain have not been fully opened, resulting in suboptimal swelling of the polymer chain.

When the density of the calcium bromide brine reached 1.75 g/cm$^3$, a substantial accumulation of calcium and bromide ions occurred around the A-DDAS copolymer chains. This abundance of ions completely shielded the attractive forces between the positive and negative charge groups on the copolymer chains, facilitating the maximum extension of the copolymer chains. Simultaneously, the extremely high concentration of calcium ions effectively attracted the free water molecules in the brine to the vicinity of the A-DDAS copolymer chains, further enhancing the swelling of the copolymer chains. Moreover, under the action of covalent micro-crosslinking, A-DDAS formed a fully swollen three-dimensional network structure. As a result, in high-temperature and high-density brine environments, A-DDAS copolymers demonstrated outstanding properties in increasing viscosity and enhancing dynamic shear force resistance.

## 4. Conclusions

In order to improve the rheological properties of high-density calcium bromide brine completion fluids under high temperature conditions, this study synthesized a micro-crosslinked amphiphilic copolymer viscosifier (i.e., A-DDAS). Meanwhile, a copolymer (i.e., A-DDA) without zwitterionic monomers was also prepared. The molecular structure and physicochemical properties of the copolymer were systematically studied by nuclear magnetic resonance (NMR), fourier transform infrared spectroscopy (FTIR), X-ray photoelectron spectroscopy (XPS), thermogravimetric analysis (TGA), and X-ray diffraction (XRD). The rheological properties of calcium bromide brine regulated by A-DDAS copolymer were comprehensively evaluated using a HAAKE rheometer and an API six-speed viscometer. The binding energy between the copolymer and water was calculated using molecular dynamics (MD) simulation and density functional theory (DFT). The molecular morphology of the copolymer in deionized water and calcium bromide brine was observed using transmission electron microscopy (TEM) to elucidate the thickening mechanism of the copolymer. The main findings were summarized as follows:

(1) The results of TGA indicated that the copolymer structure of A-DDAS exhibited significant stability, and no significant degradation was observed before reaching a temperature of 260 °C. This excellent thermal performance endowed it with applicability in high-temperature completion fluids systems.
(2) The outcomes of the HAAKE rheological experiments revealed that, at equivalent concentrations, the viscosity of the A-DDAS copolymer aqueous solution was lower than

that of the A-DDA copolymer aqueous solution. Specifically, at a concentration of 1.0 wt%, the elastic modulus $G'$ of the A-DDAS copolymer aqueous solution was lower than its loss modulus $G''$, indicating that the solution exhibited predominantly viscous behavior. In contrast, the elastic modulus $G'$ of the A-DDA copolymer aqueous solution exceeded its loss modulus $G''$, suggesting that the solution displayed primarily elastic characteristics. Furthermore, the calcium bromide brine incorporating the A-DDAS copolymer demonstrated exceptional shear-thinning and thixotropic properties.

(3) Adding 1.0 wt% A-DDAS copolymer to a 1.75 g/cm$^3$ calcium bromide brine, after aging at 180 °C for 16 h, the apparent viscosity, plastic viscosity, and yield point of the completion fluids were 71 mPa·s, 64 mPa·s, and 7 Pa, respectively, which were significantly better than HE300 and Dristemp at the same condition.

(4) Owing to the electrostatic interactions among molecules, the polymer chains of A-DDAS underwent contraction in deionized water. This contraction leads to poor solubility and a low binding energy with water molecules. Conversely, in a high-density calcium bromide brine (1.75 g/cm$^3$), the intramolecular salt bonds dissociated, causing an increase in the hydrodynamic volume and a subsequent enhancement of the binding energy with water molecules.

(5) Within high-temperature and high-density calcium bromide brine environments, the A-DDAS copolymer exhibited outstanding visco-increasing and dynamic shear-force enhancing properties. These attributes rendered it highly suitable for extensive application in solids-free completion fluids utilized in deep and ultra-deep wells.

## CRediT authorship contribution statement

**Kai-He Lv:** Resources, Funding acquisition, Conceptualization. **Qiang Li:** Conceptualization. **Li-Li Yan:** Funding acquisition, Conceptualization. **Yong Kong:** Supervision. **Zhang-Cheng Yang:** Funding acquisition. **Yuan-Zhi Qu:** Funding acquisition, Formal analysis. **Ren Wang:** Methodology. **Jin-Sheng Sun:** Conceptualization. **Jian Li:** Investigation, Funding acquisition, Data curation, Conceptualization.

## Conflict of interest

We declare that there were no financial conflicts of interest in the experimental design, data analysis, and paper writing process of this study. In addition, there is no personal relationship that affects the rigor of the experiment, the objectivity, and authenticity of the conclusions.

## Acknowledgements

The authors greatly acknowledge the financial support from the Key R&D Program of Shandong Province (2024CXPT076), National Natural Science Foundation of China (52474022, 52288101 and 52204023), Shandong Provincial Natural Science Foundation (ZR2024QE131), China National Petroleum Corporation Technology Innovation Fund Project (2022DQ02-0304), and Fund of State Key Laboratory of Deep Oil and Gas (24CX02005A).

## References

Ajieh, M.U., Amenaghawon, N.A., Owebor, K., et al., 2023. Effect of excess viscosifier and fluid loss control additive on the rheological characteristics of water-based drilling fluid. Petrol. Sci. Technol. 41 (14), 1434–1455. https://doi.org/10.1080/10916466.2022.2092636.

Akpan, E.U., 2024. Utilizing environmentally friendly polymers as rheological control and fluid loss additives in water-based drilling muds. Geoenergy Sci. Eng. 242, 213195. https://doi.org/10.1016/j.geoen.2024.213195.

Allahvirdizadeh, P., Kuru, E., Parlaktuna, M., 2016. Experimental investigation of solids transport in horizontal concentric annuli using water and drag reducing polymer-based fluids. J. Nat. Gas Sci. Eng. 35, 1070–1078. https://doi.org/10.1016/j.jngse.2016.09.052.

Boul, P.J., Reddy, B.R., Zhang, J.L., et al., 2016. Functionalized nanosilicas as shale inhibitors in water-based drilling fluids. SPE Drill. Complet. 32 (2), 121–130. https://doi.org/10.2118/185950-PA.

Cao, J., Meng, L., Yang, Y., et al., 2017. Novel acrylamide/2-acrylamide-2-methylpropanesulfonic acid/4-vinylpyridine terpolymer as an anti-calcium contamination fluid-loss additive for water-based drilling fluids. Energy Fuel. 31 (11), 11963–11970. https://doi.org/10.1021/acs.energyfuels.7b02354.

Caulfield, M.J., Qiao, G.G., Solomon, D.H., 2002. Review. Some aspects of the properties and degradation of polyacrylamides. Chem. Rev. 102 (9), 3067–3083. https://doi.org/10.1021/cr010439p.

Chang, X., Sun, J., Xu, Z., et al., 2019. A novel nano-lignin-based amphoteric copolymer as fluid-loss reducer in water-based drilling fluids. Colloids Surf. A Physicochem. Eng. Asp. 583, 123979. https://doi.org/10.1016/j.colsurfa.2019.123979.

Chu, Q., Lin, L., 2019. Synthesis and properties of an improved agent with restricted viscosity and shearing strength in water-based drilling fluid. J. Pet. Sci. Eng. 173, 1254–1263. https://doi.org/10.1016/j.petrol.2018.10.074.

Gautam, S., Kumar, S., Kumar, Kumar, A., et al., 2024. Development of functional polymer-based clay-free HPHT drilling fluid: Effect of molecular weight and its distribution on drilling fluid performance. Geoenergy Sci. Eng. 246, 213616. https://doi.org/10.1016/j.geoen.2024.213616.

Harding, S.E., Abdelhameed, A.S., Morris, G.A., 2011. On the hydrodynamic analysis of conformation in mixed biopolymer systems. Polym. Int. 60 (1), 2–8. https://doi.org/10.1002/pi.2934.

Jeong, S.W., 2019. Shear rate-dependent rheological properties of mine tailings: Determination of dynamic and static yield stresses. Appl. Sci. Basel. 9 (22), 4744. https://doi.org/10.3390/app9224744.

Jia, H., Hu, Y., Zhao, S., et al., 2019. The feasibility for potassium-based phosphate brines to serve as high-density solid-free well-completion fluids in high-temperature/high-pressure formations. SPE J. 24 (5), 2033–2046. https://doi.org/10.2118/194008-PA.

Kazemihokmabad, P., Khamehchi, E., Kalatehno, J.M., et al., 2024. A comparative study of brine solutions as completion fluids for oil and gas fields. Sci. Rep. 14 (1), 12628. https://doi.org/10.1038/s41598-024-63303-5.

Khan, R.A., Tariq, Z., Murtaza, M., et al., 2022. Ionic liquids as completion fluids to mitigate formation damage. J. Pet. Sci. Eng. 214, 110564. https://doi.org/10.1016/j.petrol.2022.110564.

Larson, R.G., Wei, Y.F., 2019. A review of thixotropy and its rheological modeling. J. Rheol. 63 (3), 477–501. https://doi.org/10.1122/1.5055031.

Li, G., Song, X., Tian, S., et al., 2022a. Intelligent drilling and completion: A review. Engineering 18, 33–48. https://doi.org/10.1016/j.eng.2022.07.014.

Li, J., Sun, J., Lv, K., et al., 2022b. Temperature- and salt-resistant micro-crosslinked polyampholyte gel as fluid-loss additive for water-based drilling fluids. Gels 8 (5), 289. https://doi.org/10.3390/gels8050289.

Li, X., Bai, Y., Gu, D., et al., 2025. Application of graphene oxide/polymer composites as filter loss reduction agents with water-based drilling fluids. J. Appl. Polym. Sci. 142 (17), e56791. https://doi.org/10.1002/app.56791.

Mohamed, A., Salehi, S., Ahmed, R., 2021. Significance and complications of drilling fluid rheology in geothermal drilling: A review. Geothermics 93, 102066. https://doi.org/10.1016/j.geothermics.2021.102066.

Rana, A., Murtaza, M., Raza, A., et al., 2024. Application of high-density brines in drilling and completion fluids: Current insights and future perspectives. Energy Fuel. 38 (8), 6561–6578. https://doi.org/10.1021/acs.energyfuels.3c04421.

Reinoso, D., Martín-Alfonso, M.J., Luckham, P.F., et al., 2019. Rheological characterisation of xanthan gum in brine solutions at high temperature. Carbohydr. Polym. 203, 103–109. https://doi.org/10.1016/j.carbpol.2018.09.034.

Sabhapondit, A., Borthakur, A., Haque, I., 2003. Water soluble acrylamidomethyl propane sulfonate (AMPS) copolymer as an enhanced oil recovery chemical. Energy Fuel. 17 (3), 683–688. https://doi.org/10.1021/ef010253t.

Singh, R., Sharma, R., Rao, G.R., 2023. A comprehensive review on the high-density clear completion fluids for applications in HPHT well completion. Int. J. Oil Gas Coal Technol. 32 (1), 70–92. https://doi.org/10.1504/IJOGCT.2023.127337.

Singh, R., Sharma, R., Rao, G.R., 2024. Investigation of the effects of ultra-high pressure and temperature on the rheological properties of a novel high-density clear completion fluids using magnesium bromide for applications in HPHT reservoirs. Geomech. Geomech. Geophys. Geo-energ. Geo-resour. 10 (1), 9. https://doi.org/10.1007/s40948-023-00724-y.

Skadsem, H.J., Leulseged, A., Cayeux, E., 2019. Measurement of drilling fluid rheology and modeling of thixotropic behavior. Appl. Rheol. 29 (1), 1–11. https://doi.org/10.1515/arh-2019-0001.

Sun, J., Chang, X., Lv, K., et al., 2020. Salt-responsive zwitterionic copolymer as tackifier in brine drilling fluids. J. Mol. Liq. 319, 114345. https://doi.org/10.1016/j.molliq.2020.114345.

Tariq, Z., Kamal, M.S., Mahmoud, M., et al., 2020. Polyoxyethylene quaternary ammonium Gemini surfactants as a completion fluid additive to mitigate

formation damage. SPE Drill. Complet. 35 (4), 696–706. https://doi.org/10.2118/201207-pa.
Wang, J., Sun, J., Huang, X., et al., 2024. A salt-responsive amphoteric viscosifier for high-density solid-free completion fluids with high temperature resistance, strong solubility, and high viscosity enhancement. Geoenergy Sci. Eng. 243, 213303. https://doi.org/10.1016/j.geoen.2024.213303.
Xiao, S., Ren, B., Huang, L., et al., 2018. Salt-responsive zwitterionic polymer brushes with anti-polyelectrolyte property. Curr. Opin. Chem. Eng. 19, 86–93. https://doi.org/10.1016/j.coche.2017.12.008.
Xie, B., Ting, L., Zhang, Y., et al., 2018. Rheological properties of bentonite-free water-based drilling fluids with novel polymer viscosifier. J. Pet. Sci. Eng. 164, 302–310. https://doi.org/10.1016/j.petrol.2018.01.074.
You, F.C., Zeng, J., Gong, C.W., et al., 2024. Experimental study of a degradable solid-free drill-in fluid system and its reservoir protection mechanism. SPE J. 29 (3), 1337–1349. https://doi.org/10.2118/218388-pa.